

Helical superconducting edge modes from pseudo-Landau levels in graphene

Daniel Sabsovich,¹ Marc W. Bockrath,² Kirill Shtengel,³ and Eran Sela¹

¹*Raymond and Beverly Sackler School of Physics and Astronomy, Tel Aviv University, Tel Aviv 69978, Israel*

²*Department of Physics, The Ohio State University, Columbus, OH 43210, USA*

³*Department of Physics and Astronomy, University of California at Riverside, Riverside, California 92521, USA*

We explore Andreev states at the interface of graphene and a superconductor for a uniform pseudo-magnetic field. Near the zeroth-pseudo Landau level, we find a topological transition as a function of applied Zeeman field, at which a gapless helical mode appears. This 1D mode is protected from backscattering as long as intervalley- and spin-flip scattering are suppressed. We discuss a possible experimental platform to detect this gapless mode based on strained suspended membranes on a superconductor, in which dynamical strain causes charge pumping.

PACS numbers: 74.50.+r, 74.45.+c, 61.48.Gh, 71.23.An

I. INTRODUCTION

Synthetic gauge fields resulting from strain [1–3] have been observed in numerous experiments on graphene samples [4–6]. These gauge fields result from the movement of the Dirac points in momentum space, which results from the modification of the hopping amplitudes by strain [7, 8]. This phenomena is general for Dirac materials [9–14] and results in time-reversal symmetric pseudo-Landau levels (LLs). In various geometries of graphene membranes, it is possible to engineer strain to yield uniform pseudo-magnetic fields

Since pseudo-magnetic fields act oppositely on the two valleys of graphene, they may have a distinct interplay with superconductivity [15–22]. A usual superconducting order parameter involving pairing of time-reversal partners, is blind to such a field. Nevertheless, the microscopic theory, critical temperature and quasiparticle excitations are strongly affected by a pseudo-magnetic field.

In this paper we explore 1D Andreev modes that can be stabilized on the interface between strained graphene and a superconductor [23, 24]. In the presence of real magnetic field Akhmerov and Beenaker [25] found cyclotron orbits of Andreev reflected electrons and holes which are fully localized when the chemical potential lies at the Dirac point, see Fig. 1(a). Physically, a specular-reflected hole [24] proceeds along the mirror-reflected segment of the electronic cyclotron trajectory. In the case of a pseudo-magnetic field, Gunawardana and Uchoa [26] found propagating states instead; see Fig. 1(b). By performing a mirror transformation to the hole trajectories and recalling that the pseudo-magnetic field has opposite signs for the two valleys, those solutions become snake states, propagating on interfaces at which a magnetic field changes sign.

Here we study the interplay of the pseudo-magnetic field B and a Zeeman magnetic field B_Z on the graphene-superconductor interface. We show that as B_Z exceeds the chemical potential μ as measured from the Dirac point, the 1D interface becomes gapless, hosting a helical 1D mode, see Fig. 1(c). Helical modes consist of counter propagating Dirac fermions carrying opposite spin, as re-

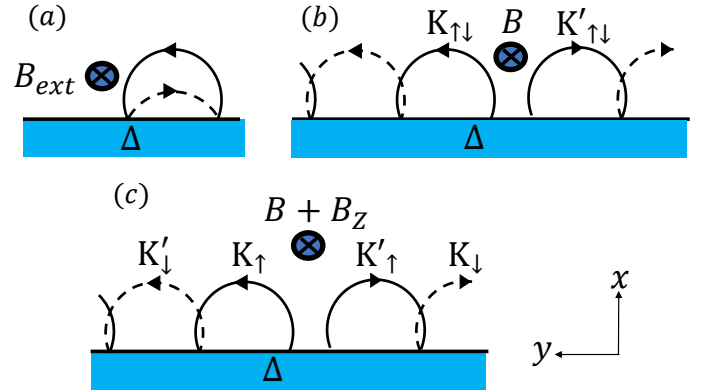


FIG. 1. (Color online) (a) Andreev interface modes for graphene near the neutrality point, for a real magnetic field B_{ext} [25], or (b) for a pseudo magnetic field B [26]. (c) With an additional Zeeman field B_Z an Andreev helical mode is stabilized.

alized on the edge of a 2D topological insulator [27] or in the zeroth Landau level in graphene by applying a Zeeman field [28, 29]. In our superconductor - strained graphene interface, the helical modes appearing due to the Zeeman field are gapless Andreev states, protected from backscattering as long as (i) disorder is smooth and does not invoke intervalley scattering and (ii) spin flip is not possible. By contrast, in the case of a real magnetic field, superconducting pairing leads to gapping of the helical edge modes, providing a platform for hosting Majorana zero modes at the boundaries of superconducting domains [30].

The paper is organized as follows. In Sec. II we solve the BdG equations describing graphene within the Dirac theory in the presence of a pairing potential step and pseudo-magnetic field. We explore in detail the low energy part undergoing a phase transition in Sec. III by projecting down to the zeroth LL and treating superconductivity, Zeeman field, and also spin-orbit coupling, as perturbations. In Sec. IV we discuss a Thouless pumping experiment, taking place as the flux associated with the pseudo-magnetic field varies in time. We conclude in Sec. V.

II. INTERFACE MODES

We consider a graphene sheet subjected to a uniform pseudo-magnetic field B , proximitized by a superconductor covering the $x < 0$ region, see Fig. 1(c). We write the Bogoliubov–de Gennes (BdG) equation as

$$\begin{bmatrix} H - \mu & \Delta(x) \\ \Delta(x)^* & \mu - THT^{-1} \end{bmatrix} \Psi = \varepsilon \Psi, \quad (1)$$

where $\Delta(x) = \Delta$ for $x < 0$ and $\Delta(x) = 0$ for $x > 0$. T here is the time-reversal operator while μ is the chemical potential. The 8×8 Hamiltonian H is decomposed as $H = H_0 + H_Z$, where H_0 describes the graphene and H_Z is a Zeeman term. Each piece can be written in terms of Pauli matrices τ, σ and s acting in valley, pseudo-spin, and spin spaces, respectively. In the valley-symmetric notation [25], graphene in a pseudo-magnetic field is described by the Hamiltonian

$$H_0 = v_F \sum_{i=x,y} (p_i \tau_0 \otimes \sigma_i + A_i \tau_3 \otimes \sigma_i) \otimes s_0. \quad (2)$$

Written explicitly in valley space, it reads

$$H_0 = v_F \begin{pmatrix} (\mathbf{p} + \mathbf{A}) \cdot \boldsymbol{\sigma} & 0 \\ 0 & (\mathbf{p} - \mathbf{A}) \cdot \boldsymbol{\sigma} \end{pmatrix} \otimes s_0. \quad (3)$$

Even in the presence of the pseudo-magnetic field, H_0 is time-reversal symmetric, $H_0 = TH_0T^{-1}$. Here $T = -i\tau_y\sigma_y s_y C$ where C denotes complex conjugation, satisfying $T^2 = -1$. On the other hand $H_Z = B_Z\tau_0 \otimes \sigma_0 \otimes s_z$ describes a Zeeman field, which is time reversal odd, $H_Z = -TH_ZT^{-1}$.

In what follows, we use the Landau gauge $\mathbf{A} = Bx\hat{y}$. An eigenvector of Eq. (3) in the K valley can be written as $\phi_K e^{ip_y y}$ where the 2-spinor $\phi_K(x)$ satisfies

$$v_F [\hbar(-i\partial_x)\sigma_x + (p_y + Bx)\sigma_y] \phi_K = \varepsilon \phi_K. \quad (4)$$

We measure length in units of magnetic length $\ell_B = \sqrt{\hbar/eB}$ and energy in units of $\hbar v_F/\ell_B$. The 2-spinor solutions are

$$\begin{aligned} \Phi_K^{(n)} &= e^{-\frac{1}{2}\xi_+^2} \begin{pmatrix} -i\sqrt{2n}H_{n-1}(\xi_+) \\ \pm H_n(\xi_+) \end{pmatrix}_{\varepsilon=\pm\sqrt{2n}}, \\ \Phi_{K'}^{(n)} &= e^{-\frac{1}{2}\xi_-^2} \begin{pmatrix} \pm H_n(\xi_-) \\ -i\sqrt{2n}H_{n-1}(\xi_-) \end{pmatrix}_{\varepsilon=\pm\sqrt{2n}}, \end{aligned} \quad (5)$$

where $\xi_{\pm} = x \pm p_y$ and $H_n(x)$ are Hermite polynomials. As detailed in the appendix, we proceed by using these solutions for the normal region $x > 0$ and imposing a boundary condition describing Andreev reflection [25, 31], valid when the superconducting coherence length is smaller than ℓ_B .

The dispersion relation $\varepsilon(p_y)$ is plotted in Fig. 2. p_y determines position along the x -axis; for $K(K')$ electrons the wave function is localized near $x = -p_y(x = p_y)$.

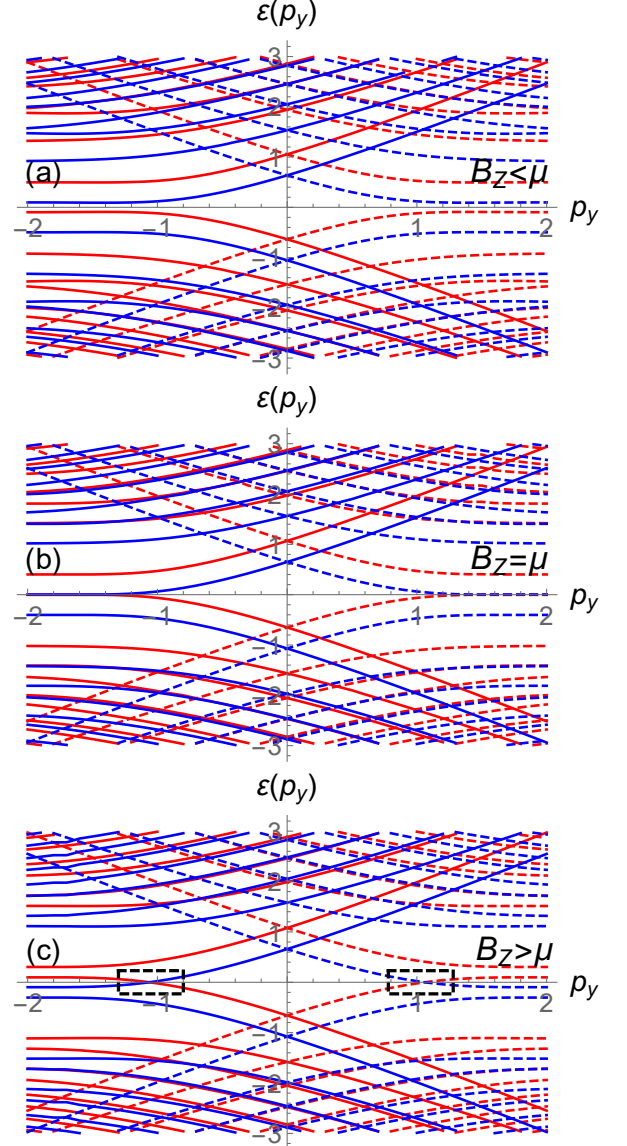


FIG. 2. (Color online) Dispersion relation $\varepsilon(p_y)$ of Andreev states at a 1D interface between proximitized graphene and normal graphene with pseudo-LLs, obtained by solving Eq. (A8) for $\Delta = 10$, $B_Z = 0.2$. We use red/blue to describe opposite spins, and full/dashed lines to describe opposite valleys. In (a) we have $\mu = 0.3$ leading to a gap, in (b) $\mu = 0.2$ the gap closes, and in (c) $\mu = 0.1$ leading to the appearance of gapless interface modes, as marked by the dashed rectangles.

Solid lines represent valley- K electron states, which for negative momentum approach the $\pm\sqrt{2n}$ values of the LLs for $B_Z = \mu = 0$, and correspond to states localized in the normal region. For increasing p_y , the modes acquire a dispersion due to the pairing potential $\Delta(x)$ setting in upon entering the superconducting region. The opposite p_y - x relationship applies for K' states (dashed lines).

This model has two phases in the $\mu - B_Z$ plane. For $|\mu| < |B_Z|$, we have gapless 1D interface modes, as seen in Fig. 2(c). By contrast, for $|\mu| > |B_Z|$, the interface is gapped, as seen in Fig. 2(a). At the transition $|\mu| = |B_Z|$

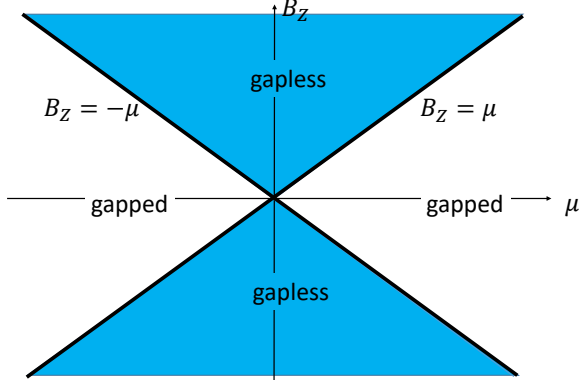


FIG. 3. (Color online) Phase diagram of our superconductor-normal (SN) interface for B_Z, μ smaller than the LL spacing.

(see Fig. 2(b)) the LL excitation gap closes at the normal side. The corresponding phase diagram is shown in Fig. 3 for the regime where μ and B_Z are small compared to the LL separation $\hbar v_F/\ell_B$. Below we focus on this low energy part by restricting the theory to the zeroth LL.

III. PROJECTION TO THE ZEROTH PSEUDO-LL

We proceed by projecting the Hamiltonian to the zeroth pseudo-LL. This approach is valid for $B_Z, \mu, \Delta \ll \hbar v_F/\ell_B$. The normalized zero energy solutions of H_0 in Eq. (5) are

$$\Phi_K^{(n=0)} = \frac{1}{\pi^{1/4}} e^{-\frac{1}{2}\xi_+^2} \begin{pmatrix} 0 \\ 1 \end{pmatrix}, \quad \Phi_{K'}^{(n=0)} = \frac{1}{\pi^{1/4}} e^{-\frac{1}{2}\xi_-^2} \begin{pmatrix} 1 \\ 0 \end{pmatrix}. \quad (6)$$

We note that we use the valley-symmetric notation in which the two sublattices are interchanged for valley K' . For a given p_y the dimension of the degenerate zero energy space of the BdG matrix Eq. (1) is 8, which includes an additional duplication due to particles and holes. We introduce a basis $|\tau^z, s^z, \eta^z\rangle$ ($\tau^z, s^z, \eta^z = \pm$) denoting the valley, spin, and particle-hole spaces, respectively. Equivalently we can use the Bogoliubov spinor

$$\Psi = (\psi_{K\uparrow}, \psi_{K\downarrow}, \psi_{K'\uparrow}, \psi_{K'\downarrow}, \psi_{K\downarrow}^\dagger, \psi_{K\uparrow}^\dagger, \psi_{K'\downarrow}^\dagger, \psi_{K'\uparrow}^\dagger), \quad (7)$$

whose eight components are defined in the basis $|\tau^z, s^z, \eta^z\rangle$ as

$$\begin{aligned} & |+++ \rangle, |+-+\rangle, |-++ \rangle, |--+\rangle, \\ & |++-\rangle, |+-\rangle, |-+-\rangle, |--\rangle \equiv |1\rangle, \dots |8\rangle; \end{aligned} \quad (8)$$

This is the basis in which the BdG matrix Eq. (1) acts.

Within this subspace H_Δ has matrix elements

$$\begin{aligned} \langle +s^z \mp | \mathcal{H}_\Delta | +s^z \pm \rangle &= \Delta \int_{-\infty}^0 \frac{1}{\sqrt{\pi}} e^{-(x+p_y)^2} dx \equiv \Delta F(p_y), \\ \langle -s^z \mp | \mathcal{H}_\Delta | -s^z \pm \rangle &= \Delta F(-p_y). \end{aligned} \quad (9)$$

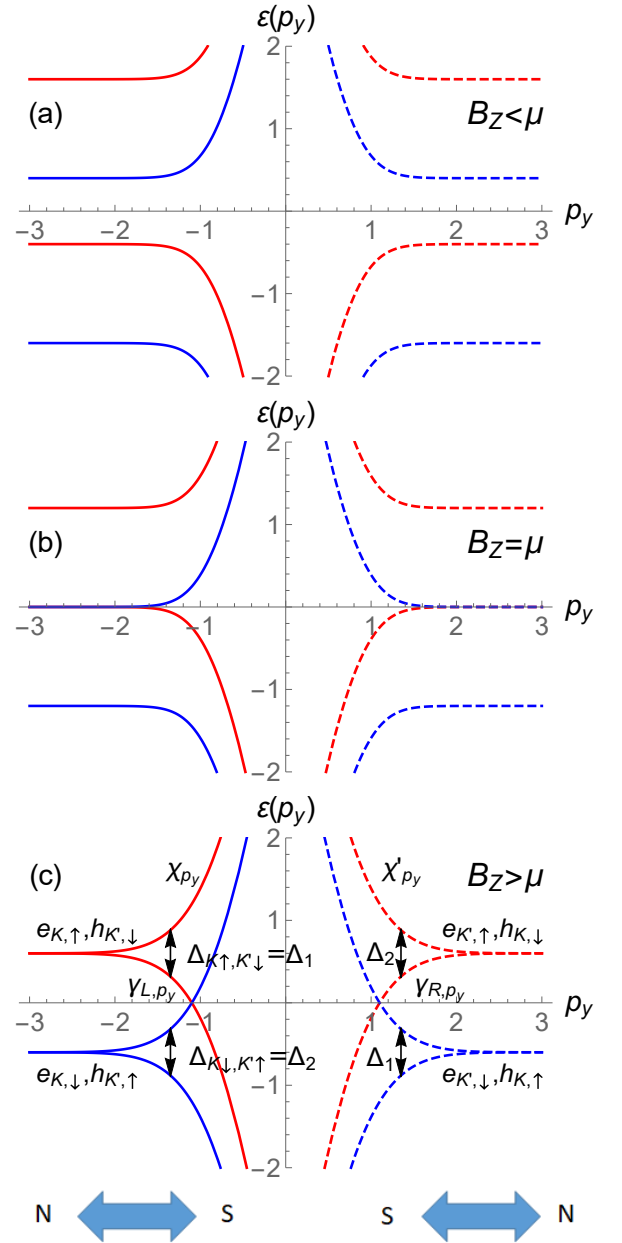


FIG. 4. (Color online) Dispersion relation of our SN interface (as in Fig. 3) focusing on the zeroth pseudo-LL using Eq. (12), setting $\Delta = 10$, $B_Z = 0.6$. In (a) $\mu = 1$ and we have a gapped interface. As we decrease μ the gap decreases and eventually closes in (b) at $\mu = 0.6$. The condition $\mu < B_Z$ leads to a gapless helical Dirac fermion as seen in (c) where $\mu = 0$. At the bottom we illustrate the $x - p_y$ relationship.

The function $F(p_y)$, describing the matrix element of the pairing potential in a state with momentum p_y , behaves as $F(p_y) \rightarrow 1$ for $p_y \rightarrow \infty$ and $F(p_y) \cong \frac{e^{-p_y^2}}{2\sqrt{\pi}|p_y|}$ for $p_y \rightarrow -\infty$. Physically, for positive p_y the support of wave functions in Eq. (6) corresponding to valley K is well within the superconductor, while for negative p_y it is mainly in the normal region. In the latter case the wave functions are affected by the pairing potential only

through their exponential tail. Hence,

$$\mathcal{H}_\Delta(p_y) = \frac{\Delta}{2} [F(p_y)(\tau_0 + \tau_z) + F(-p_y)(\tau_0 - \tau_z)] \otimes s_0 \otimes \eta_x. \quad (10)$$

The Zeeman term takes the form

$$\mathcal{H}_Z(p_y) = B_Z \tau_0 \otimes s_z \otimes \eta_0. \quad (11)$$

The eigenvalues of the projected zeroth-LL Hamiltonian

$$\mathcal{H}_{0LL}(p_y) = \mathcal{H}_Z(p_y) + \mathcal{H}_\Delta(p_y) - \mu \eta_z \quad (12)$$

are plotted in Fig. 4 for various values of B_Z and μ , reproducing the low energy sector seen in Fig. 2.

Let us focus on the 4 solutions at very negative p_y which become unaffected by Δ . They originate from electrons in valley K or holes of valley K' (non dashed). Their energies are

$$\begin{aligned} \varepsilon_1(e_{K\uparrow}) &= B_Z - \mu - \lambda_I, \\ \varepsilon_2(e_{K\downarrow}) &= -B_Z - \mu + \lambda_I, \\ \varepsilon_5(h_{K'\downarrow}) &= B_Z + \mu + \lambda_I, \\ \varepsilon_6(h_{K'\uparrow}) &= -B_Z + \mu - \lambda_I. \end{aligned} \quad (13)$$

We will introduce and discuss the role of the spin-orbit coupling λ_I in Sec. III B; for now we set $\lambda_I = 0$. Here the subscripts refer to components of the Bogoliubov spinor Ψ , see Eqs. (7) and (8). We can see that Δ separately couples modes 1 and 5 ($K \uparrow$ and $K' \downarrow$) as marked by red curves which avoid each other as p_y increases, and similarly 2 and 6 ($K \downarrow$ and $K' \uparrow$) as seen by the blue avoiding curves. Let us denote the latter level repulsions by $\Delta_{1,2}$, respectively. As can be seen in Fig. 4(c), in the topological phase $|B_Z| > \mu$ this level repulsion leads to zero energy edge states.

Consider the left moving gapless quasiparticles denoted γ_L originating from the $p_y < 0$ region due to the Δ_1 sector in Fig. 4(c). Along with the gapped partner denoted χ , this pair [red solid curves in Fig. 4(c)] can be expressed as a combination of $\psi_{K\uparrow,p}$ and $\psi_{K'\downarrow,-p}^\dagger$ in the form

$$\begin{aligned} \text{gapless} : \gamma_{L,p_y} &= u_{p_y} \psi_{K\uparrow,p_y} + v_{p_y} \psi_{K'\downarrow,-p_y}^\dagger, \\ \text{gapped} : \chi_{p_y} &= -v_{p_y} \psi_{K\uparrow,p_y} + u_{p_y} \psi_{K'\downarrow,-p_y}^\dagger. \end{aligned} \quad (14)$$

Similarly, consider the red dashed pair of curves in Fig. 4(c) forming the Δ_2 sector. They lead to a right moving gapless mode γ_R , and a gapped mode denoted χ' , which take the form

$$\begin{aligned} \text{gapless} : \gamma_{R,p_y} &= u'_{p_y} \psi_{K'\uparrow,p_y} + v'_{p_y} \psi_{K\downarrow,-p_y}^\dagger, \\ \text{gapped} : \chi'_{p_y} &= -v'_{p_y} \psi_{K'\uparrow,p_y} + u'_{p_y} \psi_{K\downarrow,-p_y}^\dagger. \end{aligned} \quad (15)$$

We emphasize that these 1D modes are Dirac- rather than Majorana-fermions. Namely $\gamma_L \neq \gamma_L^\dagger$ and $\gamma_R \neq \gamma_R^\dagger$.

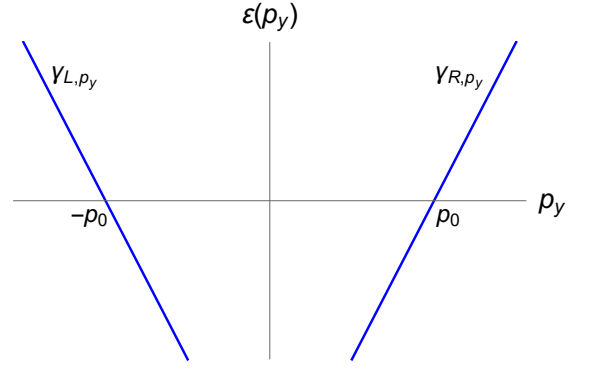


FIG. 5. Low energy spectrum describing the helical Dirac mode. the right and left moving excitations are described in Eqs. (14-15), and the Dirac Hamiltonian is given in Eq. (16).

Considering for example γ_R in the $p_y > 0$ region (red-dashed), given in Eq. (15), and applying hermitian conjugation, one obtains the right moving gapless mode in the $p_y < 0$ region (blue-solid). Thus we have both particle and hole excitations, formed out of the quasiparticle operators, allowing to define Dirac fermions. Linearizing the spectrum near $\varepsilon = 0$, the low energy Hamiltonian is then

$$H_{\text{Dirac}} = v_0 \sum_{p_y} \left[(p_y - p_0) \gamma_{R,p_y}^\dagger \gamma_{R,p_y} - (p_y + p_0) \gamma_{L,p_y}^\dagger \gamma_{L,p_y} \right]. \quad (16)$$

It is valid for energies low compared to $\min\{\varepsilon_1, \varepsilon_2, \varepsilon_5, \varepsilon_6\}$, see Eq. (13).

A. $\mathbb{Z}_2 \times \mathbb{Z}_2$ symmetry

Proximity-induced superconductivity $\sum_i \Delta c_{i\uparrow}^\dagger c_{i\downarrow}^\dagger$ breaks the $U(1)$ charge conservation down to down to \mathbb{Z}_2 , the parity conservation:

$$P = e^{i\pi \sum_{j,\sigma} c_{j,\sigma}^\dagger c_{j,\sigma}}. \quad (17)$$

At energy sufficiently low compared to the graphene's band width, the pairing Hamiltonian becomes $\int dr [\Delta_1 \psi_{K\uparrow}^\dagger \psi_{K'\downarrow}^\dagger + \Delta_2 \psi_{K'\uparrow}^\dagger \psi_{K\downarrow}^\dagger + h.c.]$, with the two terms accounting for the two valleys at opposite momenta. While $\Delta_1 = \Delta_2 = \Delta$, this form emphasizes that we have two conserved parities,

$$\begin{aligned} P_1 &= e^{i\pi \int d^2 r (\psi_{K\uparrow}^\dagger \psi_{K\uparrow} + \psi_{K'\downarrow}^\dagger \psi_{K'\downarrow})}, \\ P_2 &= e^{i\pi \int d^2 r (\psi_{K\downarrow}^\dagger \psi_{K\downarrow} + \psi_{K'\uparrow}^\dagger \psi_{K'\uparrow})}. \end{aligned} \quad (18)$$

This $\mathbb{Z}_2 \times \mathbb{Z}_2$ symmetry applies as long as the following two processes are suppressed: inter-valley scattering, $H_{i-v} = V_{iv} \sum_{\sigma,p_y} \psi_{K\sigma,p_y}^\dagger \psi_{K'\sigma,p_y} + h.c.$, and the

spin-flip scattering, $H_{\text{s-f}} = V_{\text{sf}} \sum_{p_y} \psi_{K'\uparrow, p_y}^\dagger \psi_{K\downarrow, p_y} + \psi_{K'\uparrow, p_y}^\dagger \psi_{K'\downarrow, p_y} + h.c.$. Both processes break the separate conservation of P_1 and P_2 down to a single \mathbb{Z}_2 symmetry corresponding to the conservation of $P_1 \cdot P_2$. Expressed in terms of the low energy quasiparticle excitations, $H_{\text{i-v}}$ becomes $H_{\text{i-v}} \sim V_{\text{iv}} \sum_{p_y} \gamma_{L, p_y}^\dagger \gamma_{R, p_y} + h.c.$. A uniform in space inter-valley scattering term does not open a gap since generally scattering between the two Dirac modes requires momentum transfer, see Fig 5. However, sufficiently short-range disorder can enable such momentum transfer, and hence backscattering. In the quasiparticle language $H_{\text{s-f}}$ becomes $H_{\text{s-f}} \sim V_{\text{sf}} \sum_{p_y} \gamma_{L, p_y}^\dagger \gamma_{R, -p_y} + h.c.$. Naively, the level crossing at $\varepsilon = 0$ would become avoided for a tilted Zeeman magnetic field away from the z axis. However this is false and the gapless mode persists independent of the direction of the field as long as a $U(1)$ conservation of the spin along some direction persists. In that case one can redefine a corresponding conserved $\mathbb{Z}_2 \times \mathbb{Z}_2$. However, as discussed in the next subsection, in the presence of spin-orbit coupling, tilting the direction of the Zeeman field does open a gap due to quasiparticle backscattering.

In general zero energy solutions to the BdG equation reflect a degeneracy between ground states with different parity. In our model, for $|B_Z| > |\mu|$ we have $\varepsilon \rightarrow 0$ quasiparticle solutions which change either P_1 (γ_L) or P_2 (γ_R), allowing us to identify 4 ground states.

It is interesting to note that the association of left movers with $\Delta_1 = \Delta_{K'\uparrow, K'\downarrow}$ and of the right movers with $\Delta_2 = \Delta_{K\downarrow, K'\uparrow}$ switches upon switching the sign of the Zeeman field.

B. Spin orbit coupling

Intrinsic spin orbit coupling (SOC) in graphene, which in the standard notation [32] takes the form $\lambda_I \tau_z \otimes \sigma_z \otimes s_z$, becomes in our valley-symmetric notation

$$H_{\text{SO}} = \lambda_I \tau_0 \otimes \sigma_z \otimes s_z. \quad (19)$$

Projecting this time-reversal symmetric term to the zeroth pseudo-LL subspace, its contribution to the BdG matrix Eq. (1), using Eq. (6), becomes

$$\mathcal{H}_{\text{SO}} = -\lambda_I \tau_z \otimes s_z \otimes \eta_z. \quad (20)$$

In the absence of SOC, the energy spectrum is independent of the direction of B_Z . Adding spin-orbit coupling and then rotating the Zeeman field away from the z axis in the topological phase gaps its edge. Indeed, in this case one can not define a $\mathbb{Z}_2 \times \mathbb{Z}_2$ symmetry. In order to obtain the helical modes we apply the Zeeman field along the SOC axis.

While the phase diagram in Fig. 3 reflects a phase transition occurring in both \mathbb{Z}_2 sectors, in the presence of SOC one can induce a phase transition separately in each sector. One can generalize the arguments about the level

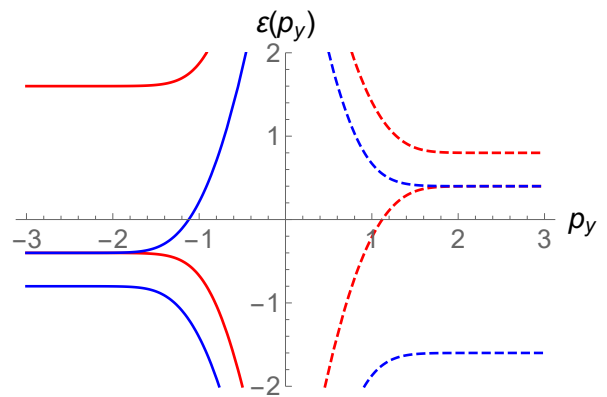


FIG. 6. (Color online) Low energy dispersion from Eq. (12) with the addition of SOC Eq. (20). Here $\Delta = 10$, $B_Z = \lambda_I = 0.6$ and $\mu = 0.4$.

repulsion due to Δ_1 or Δ_2 for the presence of SOC. In this case the energies of the four states in the normal region are given in Eq. 13 with λ_I included. The condition for the topological phase in the Δ_1 sector (Δ_2 sector) is that ε_1 and ε_5 (ε_2 and ε_6) have opposite signs. One can achieve these conditions independently. An example is shown in Fig. 6, where only the Δ_2 sector is topological, with two right-moving branches, composing one right moving chiral Dirac fermion, and no left movers. This exemplifies a quantum Hall state stabilized by a Zeeman field and SOC.

IV. PUMPING

Consider a circular geometry with the superconductor covering the region $r > R$. Imagine that the pseudo-magnetic field is uniform in space and changes in time slowly. As we explain next, in this dynamical process charge is pumped into or out of the normal region, through the NS interface.

First consider the region $\Delta = 0$ at $r < R$. dB/dt generates an azimuthal pseudo-electric field $\vec{E} = -\frac{d\vec{A}}{dt}$; Together with the pseudo-magnetic field we have a drift velocity $\vec{v}_d = \frac{\vec{E} \times \vec{B}}{|\vec{B}|^2}$ along the radial direction, see Fig. 7(a). The drift velocity has the same sign for the two valleys [33]. The resulting charge current into a region of radius r is

$$\frac{dQ(r)}{dt} = \oint_r \vec{j}(r) \cdot d\vec{l} = 2\pi r n_e e \frac{E(r)}{B}, \quad (21)$$

where we used $j = n_e e v_d$ for the inward charge current density. Assuming that the density, n_e , is determined by the filling factor ν as $n = \frac{B}{\Phi_0} \nu$, we have

$$\frac{dQ(r)}{dt} = n_e e \frac{\pi r^2 \dot{B}}{B} = e \frac{\dot{\Phi}}{\Phi_0} \nu. \quad (22)$$

Thus the change in the number of particles coincides with

ν times the change in the number of flux quanta of the pseudo-magnetic field.

Equivalently, consider the adiabatic evolution of the many-body wave function generated by \dot{B} . In the radial geometry p_y corresponds to angular momentum and is quantized, together with radius of the ring-orbitals, as

$$p_j = \frac{\hbar}{\ell_B} \sqrt{j}, \quad r_j = \ell_B \sqrt{j}, \quad j \in \mathbb{N}. \quad (23)$$

The values of p_j and r_j change upon increasing B in such a way that the r_j 's become denser, see Fig. 7(b). The particle density remains locked to the instantaneous value of B according to $n_e = \frac{B}{\phi_0} \nu$.

A. Pumping through the interface

Now we discuss the role of the SN interface $r \sim R$. Does the many-body state resulting from the motion in p_y -space coincide with the instantaneous ground state? The answer is positive if the BdG spectrum of the interface is gapped, as in the trivial phase $|\mu| > |B_Z|$. However the answer is negative for $|B_Z| > |\mu|$. In this case, Fig. 7(c) represents schematically the occupation of BdG states near the left crossing in Fig. 4(c) before pumping. We can see that occupied states form only subsets of BdG bands. As the spectral flow occurs, from the superconductor to the normal region, the p_j 's move to the left. The resulting many-body state in Fig. 7(d) is an excited state.

Thus, the gapless bands at the interface influence pumping by creating excitations. While we do not treat this explicitly, relaxation will eventually occur and create dissipation. On the other hand no dissipation is expected in the gapped regime $|B_Z| < |\mu|$.

B. Possible experimental realization

Finally, we mention a possible realization of this system. On the practical level, our setup requires systems with controlled pseudo-magnetic fields. Suggestions have been made [7, 33–35] to design graphene membranes in which one can program strain, and engineer nearly uniform pseudo-magnetic fields over macroscopic distances. One platform consists of a graphene flake suspended on a triangular aperture, with the sides normal to the $\langle 100 \rangle$ crystallographic axes of the graphene membrane. In this system a few-Tesla pseudo-field can be generated over a micrometer scale by electrostatically pulling the membrane towards a gate [7]. This platform can then allow to induce pairing correlations on pseudo-LLs using a superconducting substrate.

In the same system, where the pseudo-field is controlled via a gate, one can pump electrons in and out of the membrane simply by oscillating the gate, while the nanomechanical quality factor and frequency of the mem-

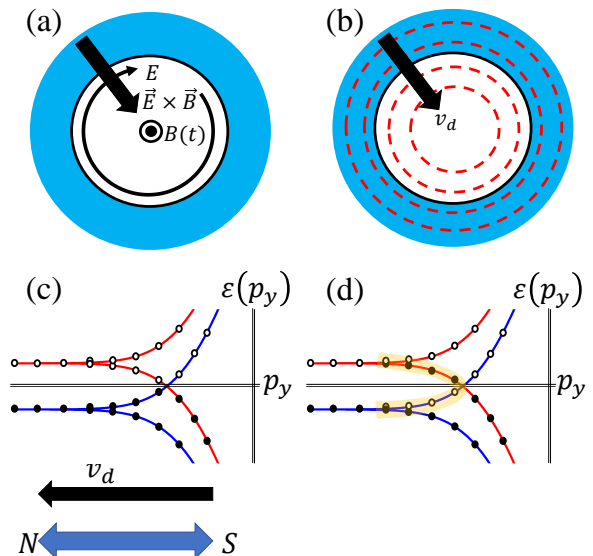


FIG. 7. (Color online) Charge pumping: (a) Circular NS interface with a time dependent pseudo-magnetic field \dot{B} creating a pseudo-electric field E . The crossed E and B pseudo-fields result [33] in a radial charge current. (b) Ring-like LL solutions adiabatically shrink as B increases. (c) Quantized momenta and their occupation in the instantaneous ground state. These bands correspond to the left side ($p_y < 0$) of Fig. 5(c). The black arrow denotes the drift in p_y as B increases. In the $p_y > 0$ region the drift is in the opposite direction in momentum space, and in the same spatial direction, not shown. (d) Excited state resulting from pumping. Marked are excited single-quasiparticle states within the gapless helical branch.

brane could potentially be detected using approaches such as those in Ref. [36]. The charge pumping itself can be detected via a shift of the mechanical resonance frequency. We leave an explicit treatment of pumping in this device for a future study.

V. CONCLUSIONS

We studied the 1D interface between strained graphene with a pseudo-magnetic field and a superconductor. Adding a Zeeman magnetic field, we identified a phase that supports helical edge modes. They are protected by a $\mathbb{Z}_2 \times \mathbb{Z}_2$ symmetry, reflecting the separate conservation of either (K, \uparrow) and (K', \downarrow) electrons, or of (K', \uparrow) and (K, \downarrow) electrons. This emergent symmetry of proximitized graphene becomes exact when intervalley and spin-flip scatterings are suppressed. SOC allows to eliminate either the right-going or the left-going edge modes, resulting in a chiral edge mode.

We note that recently there have been numerous experiments exploring the interface of graphene with superconductors, in the presence of real magnetic fields [37–43]. We discussed a possible experimental realization of a pseudo-magnetic field in a strained membrane

that would allow one to probe the predicted edge states. We demonstrated that in our time-reversal symmetric LLs AC modulation of the pseudo-field results in charge pumping. This charge pumping can flow from the superconductor to the normal region in a non-dissipative way as long as the interface is gapped. When the low energy states are present, however, as can be controlled by the Zeeman field, we argued that they will lead to dissipation.

VI. ACKNOWLEDGEMENTS

E.S and K. S. were supported by the US-Israel Binational Science Foundation (Grant No. 2016255). E. S. acknowledges support from ARO (W911NF-20-1-0013) and the Israel Science Foundation grant number 154/19. D.S is supported by the Israel Science Foundation grant No. 1790/18. M.B. is supported by the National Science Foundation grant DMR-2004801. The authors would like to thank Roni Ilan for useful discussions.

-
- [1] N. Levy, S. Burke, K. Meaker, M. Panlasigui, A. Zettl, F. Guinea, A. C. Neto, and M. Crommie, *Science* **329**, 544 (2010).
- [2] Y. Jiang, J. Mao, J. Duan, X. Lai, K. Watanabe, T. Taniguchi, and E. Y. Andrei, *Nano Lett.* **17**, 2839 (2017).
- [3] P. Nigge, A. C. Qu, É. Lantagne-Hurtubise, E. Mårzell, S. Link, G. Tom, M. Zonno, M. Michiardi, M. Schneider, S. Zhdanovich, G. Levy, U. Starke, C. Gutiérrez, D. Bonn, S. A. Burke, M. Franz, and A. Damascelli, *Sci. Adv.* **5** (2019).
- [4] K. S. Novoselov, A. K. Geim, S. V. Morozov, D. Jiang, M. I. Katsnelson, I. V. Grigorieva, S. V. Dubonos, and A. A. Firsov, *Nature* **438**, 197 (2005).
- [5] Y. Zhang, Y.-W. Tan, H. L. Stormer, and P. Kim, *Nature* **438**, 201 (2005).
- [6] A. H. Castro Neto, F. Guinea, N. M. R. Peres, K. S. Novoselov, and A. K. Geim, *Rev. Mod. Phys.* **81**, 109 (2009).
- [7] F. Guinea, M. I. Katsnelson, and A. K. Geim, *Nat. Phys.* **6**, 30 (2010).
- [8] M. A. Vozmediano, M. Katsnelson, and F. Guinea, *Phys. Rep.* **496**, 109 (2010).
- [9] D. Pikulin, A. Chen, and M. Franz, *Phys. Rev. X* **6**, 041021 (2016).
- [10] A. G. Grushin, J. W. Venderbos, A. Vishwanath, and R. Ilan, *Phys. Rev. X* **6**, 041046 (2016).
- [11] R. Ilan, A. G. Grushin, and D. I. Pikulin, *Nat. Rev. Phys.* **2**, 29 (2020).
- [12] E. Gorbar, V. Miransky, I. Shovkovy, and P. Sukhachov, *Phys. Rev. B* **96**, 125123 (2017).
- [13] V. Arjona and M. A. Vozmediano, *Phys. Rev. B* **97**, 201404 (2018).
- [14] S. Kamboj, P. S. Rana, A. Sirohi, A. Vasdev, M. Mandal, S. Marik, R. P. Singh, T. Das, and G. Sheet, *Phys. Rev. B* **100**, 115105 (2019).
- [15] P. Ghaemi, J. Cayssol, D. N. Sheng, and A. Vishwanath, *Phys. Rev. Lett.* **108**, 266801 (2012).
- [16] B. Uchoa and Y. Barlas, *Phys. Rev. Lett.* **111**, 046604 (2013).
- [17] B. Roy and V. Juričić, *Phys. Rev. B* **90**, 041413 (2014).
- [18] B. Amorim, A. Cortijo, F. de Juan, A. Grushin, F. Guinea, A. Gutiérrez-Rubio, H. Ochoa, V. Parente, R. Roldán, P. San-Jose, J. Schiefele, M. Sturla, and M. Vozmediano, *Phys. Rep.* **617**, 1 (2016).
- [19] S.-P. Lee, D. Nandi, F. Marsiglio, and J. Maciejko, *Phys. Rev. B* **95**, 174517 (2017).
- [20] G. Massarelli, G. Wachtel, J. Y. T. Wei, and A. Paramekanti, *Phys. Rev. B* **96**, 224516 (2017).
- [21] T. Liu, M. Franz, and S. Fujimoto, *Phys. Rev. B* **96**, 224518 (2017).
- [22] E. M. Nica and M. Franz, *Phys. Rev. B* **97**, 024520 (2018).
- [23] A. F. Andreev, *JETP* **19**, 1228 (1964).
- [24] C. Beenakker, *Phys. Rev. Lett.* **97**, 067007 (2006).
- [25] A. Akhmerov and C. Beenakker, *Phys. Rev. Lett.* **98**, 157003 (2007).
- [26] K. Gunawardana and B. Uchoa, *Phys. Rev. B* **91**, 241402 (2015).
- [27] M. König, S. Wiedmann, C. Brüne, A. Roth, H. Buhmann, L. W. Molenkamp, X.-L. Qi, and S.-C. Zhang, *Science* **318**, 766 (2007).
- [28] D. A. Abanin, P. A. Lee, and L. S. Levitov, *Phys. Rev. Lett.* **96**, 176803 (2006).
- [29] L. Veyrat, C. Déprez, A. Coissard, X. Li, F. Gay, K. Watanabe, T. Taniguchi, Z. Han, B. A. Piot, H. Sellier, and B. Sacépé, *Science* **367**, 781 (2020).
- [30] P. San-Jose, J. L. Lado, R. Aguado, F. Guinea, and J. Fernández-Rossier, *Phys. Rev. X* **5**, 041042 (2015).
- [31] M. Titov and C. W. J. Beenakker, *Phys. Rev. B* **74**, 041401 (2006).
- [32] C. L. Kane and E. J. Mele, *Phys. Rev. Lett.* **95**, 226801 (2005).
- [33] E. Sela, Y. Bloch, F. von Oppen, and M. B. Shalom, *Phys. Rev. Lett.* **124**, 026602 (2020).
- [34] F. Guinea, A. Geim, M. Katsnelson, and K. Novoselov, *Phys. Rev. B* **81**, 035408 (2010).
- [35] S. Zhu, J. A. Stroscio, and T. Li, *Phys. Rev. Lett.* **115**, 245501 (2015).
- [36] P. Weber, J. Güttinger, I. Tsioutsios, D. E. Chang, and A. Bachtold, *Nano Lett.* **14**, 2854 (2014).
- [37] F. Amet, C. T. Ke, I. V. Borzenets, J. Wang, K. Watanabe, T. Taniguchi, R. S. Deacon, M. Yamamoto, Y. Bomze, S. Tarucha, and G. Finkelstein, *Science* **352**, 966 (2016).
- [38] M. B. Shalom, M. Zhu, V. Fal'Ko, A. Mishchenko, A. Kretinin, K. Novoselov, C. Woods, K. Watanabe, T. Taniguchi, and A. Geim, *Nat. Phys.* **12**, 318 (2016).
- [39] G.-H. Lee, K.-F. Huang, D. K. Efetov, D. S. Wei, S. Hart, T. Taniguchi, K. Watanabe, A. Yacoby, and P. Kim, *Nat. Phys.* **13**, 693 (2017).
- [40] A. W. Draelos, M. T. Wei, A. Seredinski, C. T. Ke, Y. Mehta, R. Chamberlain, K. Watanabe, T. Taniguchi, M. Yamamoto, S. Tarucha, I. V. Borzenets, F. Amet, and G. Finkelstein, *J. Low Temp. Phys.* **191**, 288 (2018).

- [41] M. Zhu, M. Ben Shalom, A. Mishchenko, V. Fal'ko, K. Novoselov, and A. Geim, *Nanoscale* **10**, 3020 (2018).
- [42] K.-F. Huang, Y. Ronen, R. Mélin, D. Feinberg, K. Watanabe, T. Taniguchi, and P. Kim, (2020), arXiv:2008.03419 [cond-mat.mes-hall].
- [43] Önder Gül, Y. Ronen, S. Y. Lee, H. Shapourian, J. Zauberman, Y. H. Lee, K. Watanabe, T. Taniguchi, A. Vishwanath, A. Yacoby, and P. Kim, (2020), arXiv:2009.07836 [cond-mat.mes-hall].

Appendix A: Interface dispersion via the Akhmedrov-Beenaker method [25]

We start with a graphene Hamiltonian containing pseudo-field, intrinsic SOC and Zeeman terms in the valley isotropic basis, as described in Eqs. (3), (11) and (19), and transform it into the BdG equation in Eq. (1).

We wish to describe bound Andreev states at the SN interface, thus we follow the procedure set by [25] and start by solving Eq. (1) in the $x > 0$ normal region. The solution follows the canonical lines of pseudo LLs theory

in graphene, where we adjust for the presence of SOC and Zeeman terms. We find the eigenvectors

$$\Psi(x, y) = e^{ip_y y} \begin{pmatrix} C_e^{K, \uparrow} \Phi_e^{K, \uparrow}(\xi_+) \\ C_e^{K, \downarrow} \Phi_e^{K, \downarrow}(\xi_+) \\ C_e^{K', \uparrow} \Phi_e^{K', \uparrow}(\xi_-) \\ C_e^{K', \downarrow} \Phi_e^{K', \downarrow}(\xi_-) \\ C_h^{K', \downarrow} \Phi_h^{K', \downarrow}(\xi_+) \\ C_h^{K', \uparrow} \Phi_h^{K', \uparrow}(\xi_+) \\ C_h^{K, \downarrow} \Phi_h^{K, \downarrow}(\xi_-) \\ C_h^{K, \uparrow} \Phi_h^{K, \uparrow}(\xi_-) \end{pmatrix}, \quad (\text{A1})$$

with the spinors Φ defined as

$$\Phi_e^{K, s_z}(\xi_+) = e^{-\frac{\xi_+^2}{2}} \begin{pmatrix} -i(\mu + \varepsilon + \lambda_I s_z - B_Z s_z) \frac{H_{(\mu + \varepsilon)^2 - \lambda_I^2 - 2B_Z(\mu + \varepsilon)s_z + B_Z^2}}{2}(\xi_+) \\ H_{\frac{(\mu + \varepsilon)^2 - \lambda_I^2 - 2B_Z(\mu + \varepsilon)s_z + B_Z^2}{2}}(\xi_+) \end{pmatrix}, \quad (\text{A2})$$

$$\Phi_e^{K', s_z}(\xi_-) = e^{-\frac{\xi_-^2}{2}} \begin{pmatrix} H_{\frac{(\mu + \varepsilon)^2 - \lambda_I^2 - 2B_Z(\mu + \varepsilon)s_z + B_Z^2}{2}}(\xi_-) \\ -i(\mu + \varepsilon - \lambda_I s_z - B_Z s_z) \frac{H_{(\mu + \varepsilon)^2 - \lambda_I^2 - 2B_Z(\mu + \varepsilon)s_z + B_Z^2}}{2}(\xi_-) \end{pmatrix}, \quad (\text{A3})$$

$$\Phi_h^{K', s_z}(\xi_+) = e^{-\frac{\xi_+^2}{2}} \begin{pmatrix} -i(\mu - \varepsilon - \lambda_I s_z - B_Z s_z) \frac{H_{(\mu - \varepsilon)^2 - \lambda_I^2 - 2B_Z(\mu - \varepsilon)s_z + B_Z^2}}{2}(\xi_+) \\ H_{\frac{(\mu - \varepsilon)^2 - \lambda_I^2 - 2B_Z(\mu - \varepsilon)s_z + B_Z^2}}{2}(\xi_+) \end{pmatrix}, \quad (\text{A4})$$

$$\Phi_h^{K, s_z}(\xi_-) = e^{-\frac{\xi_-^2}{2}} \begin{pmatrix} H_{\frac{(\mu - \varepsilon)^2 - \lambda_I^2 - 2B_Z(\mu - \varepsilon)s_z + B_Z^2}}{2}(\xi_-) \\ -i((\mu - \varepsilon) + \lambda_I s_z - B_Z s_z) \frac{H_{(\mu - \varepsilon)^2 - \lambda_I^2 - 2B_Z(\mu - \varepsilon)s_z + B_Z^2}}{2}(\xi_-) \end{pmatrix}, \quad (\text{A5})$$

where $s_z = \uparrow \downarrow = \pm 1$. The bound Andreev states on the interface at $x = 0$ are described using a boundary condition equation

$$(M_{NS} - 1)\Psi = 0, \quad (\text{A6})$$

where the matrix M_{NS} is given by [25, 31]

$$M_{NS} = \tau_0 s_0 \left(\frac{\varepsilon}{\Delta} - i\sigma_x \sqrt{1 - \frac{\varepsilon^2}{\Delta^2}} \right). \quad (\text{A7})$$

This is similar to the BC equation presented in [25], where we include the constraint for transitions between electrons and holes to involve opposite spins via s_0 in Eq. (A7). Solving Eq. (A6) for the wave function in Eqs. (A1)-(A5) at $x = 0$, gives the dispersion relation $\varepsilon(p_y)$. The four solutions can be written compactly with $s_z = \pm 1$ as

$$f_{\mu - \varepsilon + s_z \lambda_I + s_z B_Z}(p_y) - f_{\mu + \varepsilon + s_z \lambda_I - s_z B_Z}(p_y) = \frac{\sqrt{\Delta^2 - \varepsilon^2}}{\varepsilon} (1 + f_{\mu + \varepsilon + s_z \lambda_I - s_z B_Z}(p_y) f_{\mu - \varepsilon + s_z \lambda_I + s_z B_Z}(p_y)) \quad (\text{A8})$$

$$f_{\mu - \varepsilon - s_z \lambda_I + s_z B_Z}(-p_y) - f_{\mu + \varepsilon - s_z \lambda_I - s_z B_Z}(-p_y) = \frac{\sqrt{\Delta^2 - \varepsilon^2}}{\varepsilon} (1 + f_{\mu + \varepsilon - s_z \lambda_I - s_z B_Z}(-p_y) f_{\mu - \varepsilon - s_z \lambda_I + s_z B_Z}(-p_y)) \quad (\text{A9})$$

where we define

$$f_{\alpha \pm \lambda_I \mp B_Z}(p_y) \equiv \frac{H_{\frac{\alpha^2 - \lambda_I^2 \mp 2B_Z \alpha + B_Z^2}{2}}(p_y)}{(\alpha \pm \lambda_I \mp B_Z) \frac{H_{\frac{\alpha^2 - \lambda_I^2 \mp 2B_Z \alpha + B_Z^2}{2}}(p_y)}{2}} \quad (\text{A10})$$

$$f_{\alpha \pm \lambda_I \pm B_Z}(p_y) \equiv \frac{H_{\frac{\alpha^2 - \lambda_I^2 \pm 2B_Z \alpha + B_Z^2}{2}}(p_y)}{(\alpha \pm \lambda_I \pm B_Z) \frac{H_{\frac{\alpha^2 - \lambda_I^2 \pm 2B_Z \alpha + B_Z^2}{2}}(p_y)}{2}} \quad (\text{A11})$$

We solve Eqs. (A8)-(A9) for ε as a function of p_y numerically to get the spectra plotted in Fig. 2.